ORGANOMETALLICS

Article

pubs.acs.org/Organometallics

Controlling the Selectivity of C−H Activation in Pyridinium Triazolylidene Iridium Complexes: Mechanistic Details and Influence of Remote Substituents

Kate F. Donnelly,[†] Ralte Lalrempuia,[†] Helge Müller-Bunz,[†] Eric Clot,*[,‡] and Martin Albrecht*[,†]

[†]School of Chemistry & Chemical Biology, University College Dublin, Belfield, Dublin 4, Ireland

[‡]Institut Charles Gerhardt, CNRS 5253, Université Montpellier 2, cc1501, Place Eugène Bataillon, 34095 Montpellier Cedex, France

Supporting Information

ABSTRACT: Iridium complexes containing a triazolylidene ligand with an appended methylpyridinium site undergo either aromatic C(sp^2)−H bond activation or exocyclic C(sp^3)−H bond activation of the N-bound methyl group. The selectivity of these bond activations is controlled by the remote substituent R of the triazolylidene ligand. Iterative computational and synthetic experiments provide evidence for more facile C(sp^2)−H bond activation for a variety of remote substituents with R = Me, $CH_2C_6F_5$, $CH_2CH_2C_6H_5$. For triazolylidene ligands with a benzylic substituent, C(sp^2)−H bond activation of this benzylic group is the lowest energy pathway and is competitive with aromatic pyridinium C−H bond activation. The generated cyclometalated species is metastable and undergoes, via an oxidative addition/reductive elimination sequence, a transcyclometalation with exclusive activation of the methyl C−H bond and thus leads to the C(sp^3)−H bond activated product. An experimental determination of activation energies as well as isomer ratios of the intermediates validates the computed pathways. The application of a transcyclometalation procedure to activate more challenging C(sp^3)−H bonds is unprecedented and constitutes an attractive concept for devising catalytic processes.

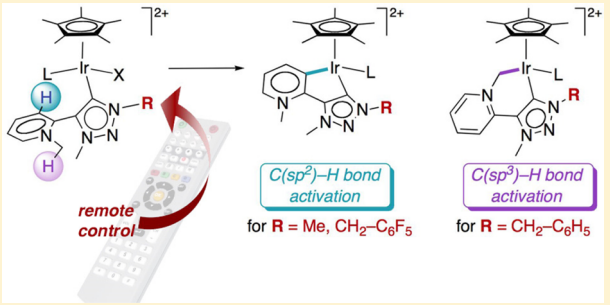

INTRODUCTION

The activation of carbon−hydrogen bonds in saturated and unsaturated hydrocarbon molecules is one of the major challenges in catalysis, with far-reaching implications for synthetic processes.[1] The development in this field is greatly incentivized by the availability of hydrocarbon feedstocks from the petrochemical industry. However, the ubiquity of C−H bonds within these molecules, while providing abundant substrates for C−H activation, poses a challenge in achieving a high degree of selectivity, which is paramount to the successful employment of this concept in organic synthesis. The advent of research into transition-metal-mediated C−H bond activation has allowed for the selective activation of specific bonds, thus providing a means of rectifying this primary issue. Transition-metal complexes that can accomplish such selective bond activations under mild conditions have become privileged catalysts for a number of organic transformations.[2,3]

Iridium complexes, in particular, have been shown to exhibit a high degree of reactivity and selectivity in C−H bond activation. Research in this area has been motivated by the original work carried out by Bergman on the intermolecular activation of alkyl C−H bonds by an iridium Cp* complex.[4] The scope of iridium-mediated C−H activations has broadened to include, for example, alkane dehydrogenation,[5,6] catalytic methane oxidation,[7,8] and catalytic H/D exchange.[9]

We previously reported that iridium complexes such as **2** and **3** comprising carbene ligands derived from triazolium salts[10] (Scheme 1) are excellent water oxidation catalyst precursors that produce very high turnover numbers.[11] The synthesis of these triazolylidene iridium complexes involves C−H bond activation of the pyridinium unit in **1a** and yields a mixture of two cyclometalated complexes, one featuring a pyridylidene ligand from C(sp^2)−H bond activation (**2a**) and the other product resulting from C(sp^3)−H bond activation (**3a**).

Intrigued by this competitive C−H bond activation process, we have explored the factors that govern the formation of **2** and **3**. Chemical modification of the triazolylidene ligand structure at the remote benzylic position surprisingly exerts a strong influence on the C(sp^2)−H vs C(sp^3)−H bond activation selectivity. The key mechanistic aspects of these C−H bond activation processes were elucidated by iterative quantum chemical and experimental investigations and underpin the unique capacity of iridium, in particular when bound to triazolylidene ligands, as a versatile platform for selective activation of (unactivated) C−H bonds.

Received: November 27, 2014

DOI: 10.1021/om501197g
Organometallics XXXX, XXX, XXX−XXX

Scheme 1. Iridation of 1a To Give the Products of C(sp^2)−H Activation, 2a, and C(sp^3)−H Activation, 3a

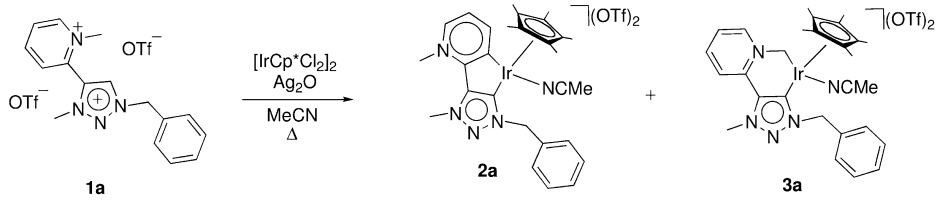

Scheme 2. Iridation of Pyridinium Triazolium Salts 1b−e

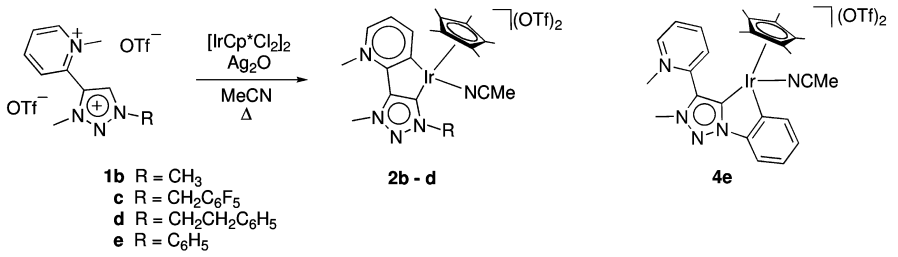

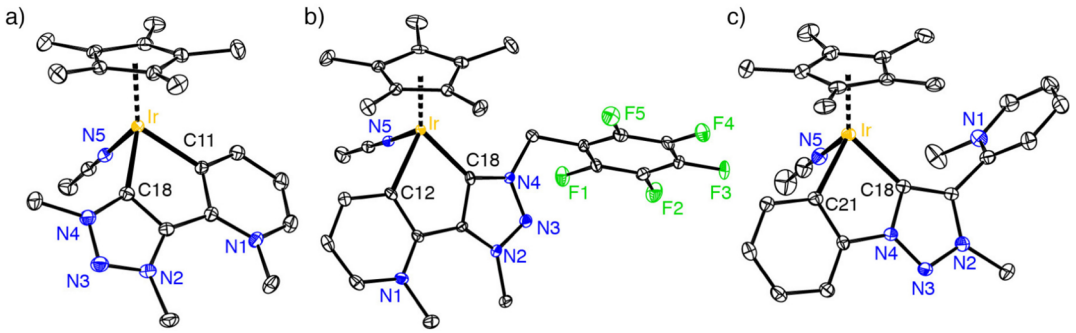

Figure 1. ORTEP representation of complexes (a) **2b** (b) **2c**, and (c) **4e** (50% probability, ⁻OTf ions and protons are omitted for clarity; structures of **2b** and **4e** from ref 12).

RESULTS AND DISCUSSION

Iridation of the triazolium salt **1b** bearing a N-bound methyl substituent in place of the benzyl group gave exclusively complex **2b** without forming any detectable quantities of the six-membered metallacycle due to C(sp^3)−H activation of the N−CH$_3$ group.[12] This initial observation indicated a particular role of the wingtip group. Hence, synthetic variation of the ligand precursor included, in particular, the modification of the wingtip group R from benzyl to the fluorinated version (**1c**), and moving the aromatic ring of the wingtip group further away from and closer to the potential triazolylidene ring (**1d,e**, respectively).

Iridation of the pyridinium triazolium salts **1b−d** produces, exclusively, complexes **2b−d** (Scheme 2). In contrast, iridation of **1e** affords the product of phenyl C(sp^2)−H activation, **4e**. Complexes **2b,c** and **4e** were fully characterized; however, only spectroscopic data are available for **2d** due to the presence of an inseparable impurity, tentatively concluded to be a doubly cyclometalated iridium complex. Spectroscopically, complexes **2b−d** share similarities, which include the loss of a pyridyl proton resonance in comparison to the starting material and the downfield shift of the Ir-bound carbenic carbon of the pyridylidene ligand at δ_C 154.0, 153.0, and 154.1 ppm for **2b−d**, respectively. The triazolylidene carbenes also appear downfield at δ_C 154.6, 155.4, and 153.7 ppm. While pyridinium C−H activation in **2b−d** was unambiguously identified by the three characteristic doublet of doublets patterns in the low-field ^{1}H NMR range, the spectrum of complex **4e** featured four pyridinium protons and a desymmetrized phenyl group due to Ir−C$_{Ph}$ bonding. The remaining four phenyl protons resonate as distinct doublets and triplets in the spectrum. The carbenic resonance of the triazolylidene is shifted downfield (δ_C 146.6 ppm), and the anionic C$_{Ph}$−Ir carbon (δ_C 144.1) is upfield with respect to the Ir-bound pyridylidene nuclei (see above). Further structural evidence of **2b**,[12] **2c**, and **4e**[12] was obtained from single-crystal X-ray diffraction analyses (Figure 1).

While iridation of **1b−e** gave a single product, metalation of **1a** afforded several complexes. The ^{1}H NMR spectrum of the crude product mixture after 18 h reaction time indicated that **2a** and **3a** are present in a 2:3 ratio. Separation of the two products was achieved due to their different solubility properties.[11] Apart from the product signals, two additional Cp* resonances are present at higher field in the ^{1}H NMR spectra of the crude mixtures, δ_H 1.57 and 1.52 ppm vs δ_H 1.80 and 1.60 ppm for **2a** and **3a**, respectively. These signals constitute the major portion in the spectrum (ca. 75 ± 10%) and were attributed to intermediates en route to C(sp^3)−H bond activation, since they transform to the ylidic complex **3a** upon purification or storage in the solid state. Such a transformation was deduced from the significantly increased yields in comparison to the spectroscopic yields initially determined from crude mixtures (see also discussion of complex **6** below). In contrast, the yield of complex **2a** did not change over time, and hence, the overall selectivity of the metalation implies an approximate 1:9

DOI: 10.1021/om501197g
Organometallics XXXX, XXX, XXX−XXX

Table 1. Selected Bond Lengths (Å) and Angles (deg) for Complexes 2b, 2c, and 4e and the Corresponding Calculated Structures $2b_{calc}$, $2c_{calc}$, and $4e_{calc}$, Respectively

	2b	$2b_{calc}$	2c	$2c_{calc}$	4e	$4e_{calc}$
Ir−C_{trz}	2.017(1)	2.014	2.020(2)	2.017	2.039(3)	2.030
Ir−$C_{pyr/Ph}$	2.049(1)	2.059	2.056(3)	2.056	2.070(4)	2.069
Ir−N	2.033(2)	2.041	2.041(2)	2.039	2.035(2)	2.033
Ir−$Cp^*_{centroid}$	1.8559(1)	1.888	1.8531(1)	1.889	1.8526(1)	1.886
C_{trz}−Ir−N	90.09(6)	90.0	86.84(9)	90.2	86.8(1)	92.0
$C_{pyr/Ph}$−Ir−N	85.21(9)	90.2	87.61(6)	89.4	85.3(1)	84.7
C_{trz}−Ir−$C_{pyr/Ph}$	76.02(6)	76.7	76.65(9)	76.7	78.4(1)	78.4

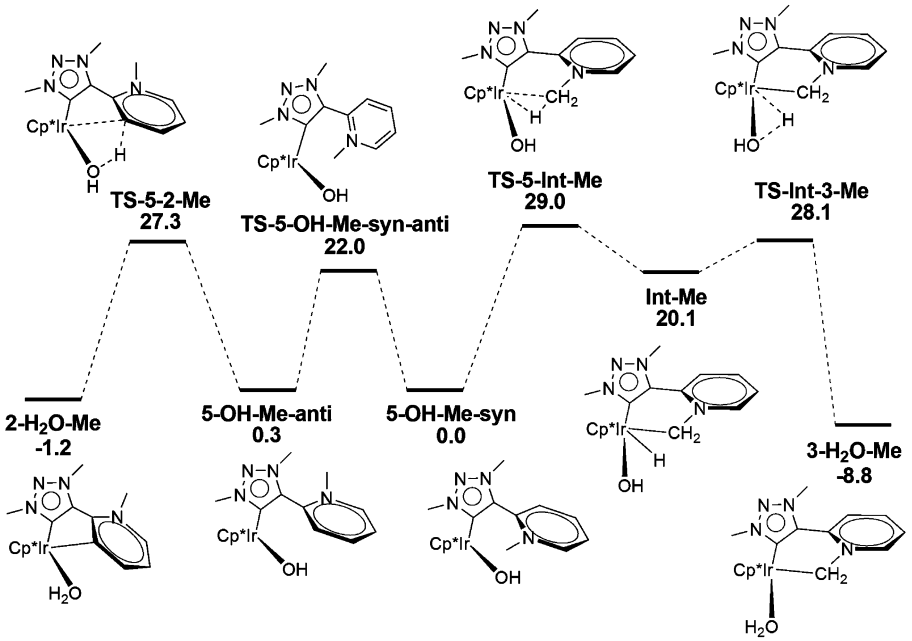

Figure 2. Reaction trajectories and Gibbs free energy profiles (in kcal mol^{-1} at 353 K) for the competitive C(sp^2)−H bond activation (left side) and C(sp^3)−H bond activation (right side) in the case R = Me.

selectivity for the formation of **2a** vs **3a**, including intermediates en route to **3a**.

Computational Study. DFT (B3PW91) calculations have been carried out to elucidate the mechanism of formation of **2** and **3** and to understand the origin of the experimental selectivity of C(sp^2)−H vs C(sp^3)−H bond activation observed as a function of triazolylidene substituents. The actual experimental partners were considered in the calculations, and all of the energy values given below (kcal mol^{-1}) are Gibbs energy values obtained as the sum of the solvent-corrected energy (smd model, MeCN), the gas-phase Gibbs correction at 353 K, and the D3(BJ) dispersion correction. As an illustration of the quality of the computational strategy, Table 1 shows a comparison of selected geometrical parameters among the X-ray structures of **2b**, **2c**, and **4e** and the corresponding optimized structures $2b_{calc}$, $2c_{calc}$, and $4e_{calc}$.[13] The agreement between the experimental and computational values is excellent.

As a starting point, formation of a monodentate iridium complex **5** after C−H activation of the triazolium cation is a conceivable first intermediate (Figure 2) that should be readily accessible in the presence of Ag_2O.[14] The monodentate complex **5-OH-Me**, bearing a hydroxide as ancillary ligand due to proton transfer from the triazolium salt to the silver oxide precursor,[15] was computed to have the lowest energy and therefore was assumed to be the relevant species that initiates the second C−H bond activation process (Figure S1 in the Supporting Information).[16] Two isomers were identified for this species, one with a syn (**5-OH-Me-syn**) and the other with an anti orientation (**5-OH-Me-anti**) of the pyridinium methyl group with respect to the hydroxide ligand (Figure 2). The stability difference of these two conformers is not especially dependent on the substituents R, and the anti orientation is in all cases slightly disfavored ($\Delta G \leq 2.0$ kcal mol^{-1}; Table 2). This value is in excellent agreement with experimental data: the NMR spectrum of the monodentate complex **5b** shows a 1:0.7 syn/anti mixture at room temperature, which corresponds to an energy difference $\Delta G = 0.24$ kcal mol^{-1}. The transition state connecting **5-OH-Me-syn** and **5-OH-Me-anti**, **TS-5-OH-syn-anti**, has been located on the potential energy surface at $\Delta G^{\ddagger} = 22.0$ kcal mol^{-1} above **5-OH-Me-syn** (Figure 2). The isomerization is associated with a rotation of the pyridinium ring that is almost coplanar with the triazole ring in the transition state structure.

The dicationic iridium(III) complex **5** is formally equivalent to $[Cp^*Ir(PMe_3)(Me)]^+$, which was shown by Bergman to be active in C−H bond activation.[17] Calculations on C−H bond activation of methane by $[CpIr(PR_3)(Me)]^+$ (R = H, Me) indicated that the pathway follows an oxidative addition/reductive elimination route, while no σ-bond metathesis pathway could be identified.[18] Similar C(sp^3)−H oxidative addition of the *N*-methyl group was located on the potential energy surface when starting from **5-OH-Me-syn** (Figure 2,

DOI: 10.1021/om501197g
Organometallics XXXX, XXX, XXX−XXX

Table 2. Gibbs Energy Values of the Extrema Located on the Pathways for 2 and 3, via C(sp^2)−H and C(sp^3)−H Bond Activation, Respectively[a]

	complex (R)			
	2a ($CH_2C_6H_5$)	**2b** (CH_3)	**2c** ($CH_2C_6F_5$)	**2e** (C_6H_5)
5-OH-R-anti	1.8	0.3	2.0	1.1
TS-5-2-R	27.4	27.3	28.1	28.7
2-H_2O-R	1.0	−1.2	1.3	0.2
2-CH_3CN-R (2_{calc})	−14.6	−22.4	−15.0	−15.6
TS-5-OH-R-syn-anti	23.3	22.0	21.9	22.5
	complex (R)			
	3a ($CH_2C_6H_5$)	**3b** (CH_3)	**3c** ($CH_2C_6F_5$)	**3e** (C_6H_5)
5-OH-R-syn	0.0	0.0	0.0	0.0
TS-5-Int-R	31.3	29.0	28.8	32.1
Int-R	23.0	20.1	21.3	25.5
TS-Int-3-R	30.7	28.1	29.7	30.9
3-H_2O-R	−7.3	−8.8	−4.8	−4.9
3-CH_3CN-R (3_{calc})	−20.7	−22.5	−21.6	−18.5

[a]Energies in kcal mol^{-1} at 353 K relative to the most stable hydroxide complex **5-OH-R-syn**.

right part). The activation barrier $\Delta G^{\ddagger}$ = 29.0 kcal mol^{-1} is rather high for observing significant reactions at 353 K (half-life of ca. 24 h). Competitive C(sp^2)−H bond activation was predicted from **5-OH-Me-anti** via a σ-bond metathesis transition state[19] **TS-5-2-Me** with a slightly lower activation barrier, $\Delta G^{\ddagger}$ = 27.0 kcal mol^{-1} (Figure 2, left part). In this transition state, the C−H bond is significantly elongated (1.324 Å) and the O−H bond is not yet formed (1.292 Å). The Ir−O bond is elongated from 1.938 Å in **5-OH-Me-anti** to 2.132 Å in the transition state **TS-5-2-Me**. The putative Ir−C bond is still much longer (2.525 Å) than that in the product **2-H_2O-Me** (2.061 Å). This transformation, where an available lone pair on a ligand is used to abstract the hydrogen atom, can be considered to be an ambiphilic metal ligand activation (AMLA) as introduced by Macgregor et al., where the process involves a four-membered ring and is thus called AMLA(4).[20] Formation of **2-H_2O-Me** is slightly exergonic with ΔG = −1.5 kcal mol^{-1}, but substitution of the aqua ligand with MeCN to afford the final complex **2-CH_3CN-Me** (i.e., **2b**$_{calc}$) is associated with a significant gain of energy, ΔG = −22.4 kcal mol^{-1}, with respect to **5-OH-Me-syn** (Table 2).

The transition state for the isomerization between **5-OH-Me-syn** and **5-OH-Me-anti** lies at lower energy than both TSs for C−H activation. The transformation is thus under Curtin−Hammett conditions, and the preferred pathway is that associated with the overall lower transition state structure. The energy of the transition state of the C(sp^2)−H bond activation via AMLA(4) (**TS-5-2-Me**) was computed to be 1.7 kcal mol^{-1} lower than the highest transition state for C(sp^3)−H bond activation (**TS-5-Int-Me**). This difference translates into a ca. 11-fold increase of the rate constant and significantly shorter reaction times (half-life time ca. 1 h vs 24 h). There is thus a strong kinetic preference to form **2b** and, considering the very high barrier computed for the reverse reaction ($\Delta G^{\ddagger}$ = 49.7 kcal mol^{-1} from **2-CH_3CN-Me** to **TS-5-2-Me**), a thermodynamic equilibrium between **2b** and **3b** is out of reach.

Calculations involving ligand precursors **1a−e** revealed similar trends. While **3-H_2O-R** is thermodynamically favored over **2-H_2O-R**, C(sp^2)−H activation and formation of **2** is kinetically preferred over C(sp^3)−H bond activation, independent of the substituent R on the triazolylidene scaffold (Table 2). The kinetic preference for C(sp^2)−H bond activation is 1.6−3.9 kcal mol^{-1}, an energy difference sufficiently large to observe exclusive formation of **2** irrespective of the nature of R. This conclusion aligns well with the experimental formation of only complexes **2b−d** upon metalation of triazolium salts **1b−d**, but fails to explain the results for the other R groups (R = Ph, Bn).

In contrast to the pyridinium C−H activation observed for **1a−d**, reaction of **1e** under identical conditions yielded the cyclometalated species **4e**, and the pyridinium fragment remained unperturbed even on heating for prolonged periods of time. Cyclometalation of the phenyl group bound to the triazolylidene at nitrogen was previously shown to be straightforward for electron-poor transition metals and was always preferred over C−H activation of the C-bound phenyl ring.[21] These experimental observations are also supported by calculations. Computation of the C(sp^2)−H activation of the N-bound phenyl ring from either the syn intermediate ($\Delta G^{\ddagger}$ = 22.4 kcal mol^{-1} from **5-OH-Ph-syn**) or the anti isomer ($\Delta G^{\ddagger}$ = 20.8 kcal mol^{-1} from **5-OH-Ph-anti**) unveiled transition states that are significantly lower than those for C(sp^2)−H or C(sp^3)−H activation of the pyridinium substituent ($\Delta G^{\ddagger} \geq$ 27.6 kcal mol^{-1}; Table 2). As in the case of C(sp^2)−H activation of the pyridinyl ring, the C(sp^2)−H activation of the N-bound phenyl substituent is an AMLA(4) process, forming coordinated water in a single step. Moreover substitution of water for MeCN in the product of C−H activation of the N-bound phenyl ring yielded complex **4-CH_3CN-Ph** (i.e., **4e**$_{calc}$) at ΔG = −20.2 kcal mol^{-1} with respect to **5-OH-Ph-syn**. This is lower in energy than the MeCN complexes **2e**$_{calc}$ and **3e**$_{calc}$ that would have resulted from C−H activation of the methylpyridinium ring (Table 2). There is thus both a kinetic and thermodynamic preference for C−H activation of the N-bound phenyl ring, in agreement with the experimental observation of **4e**.

The calculations indicate a clear stabilization of the C(sp^2)−H activation of the phenyl ring with respect to C(sp^2)−H or C(sp^3)−H activation of the pyridinium ring with $\Delta\Delta G^{\ddagger}$ values of 6.8 kcal mol^{-1} (**TS-5-2-Ph**) and 10.2 kcal mol^{-1} (**TS-5-Int-Ph**) with respect to the most stable transition state of the former process (**TS-5-4-Ph-anti**). The geometrical parameters associated with the C−H cleavage of the various transition state structures are indicative of the occurrence of different modes of activation. In the two extreme situations (**TS-5-4-Ph-anti** and **TS-5-Int-Ph**), the forming Ir···C bond distances are similar (2.291 and 2.257 Å, respectively). However, the breaking C···H bond is significantly longer in the C(sp^3)−H activation transition state (1.267 Å, **TS-5-4-Ph-anti**; 1.527 Å, **TS-5-Int-Ph**). This is accompanied by a significantly shorter Ir···H distance in **TS-5-Int-Ph** (1.590 Å) in comparison to **TS-5-4-Ph-anti** (1.991 Å), indicative of some Ir···H interaction in the former TS. Finally, there is no participation of the OH ligand in the C(sp^3)−H bond cleavage (O···H = 2.357 Å; Ir−O = 2.056 Å), whereas OH does participate in the C−H bond breaking process in **TS-5-4-Ph-anti** (O···H = 1.403 Å; Ir−O = 2.134 Å). The geometries of these two TSs support an oxidative addition pathway for C(sp^3)−H activation, whereas the C(sp^2)−H bond activation of the phenyl ring is best described as an ambiphilic metal−ligand activation, where both the metal and the ligand (OH) participate in the activation. The situation for **TS-5-2-Ph** is significantly different with a much longer Ir···C distance

DOI: 10.1021/om501197g
Organometallics XXXX, XXX, XXX−XXX

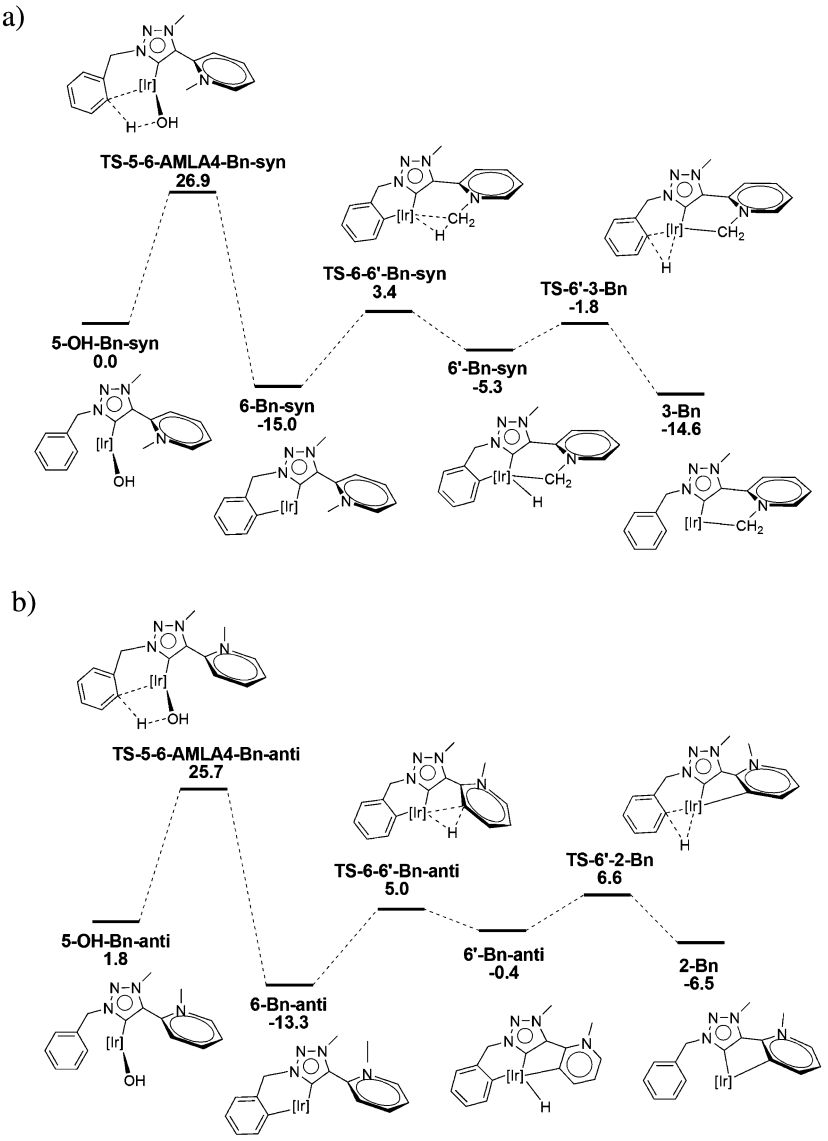

Figure 3. Gibbs energy (353 K, kcal mol^{-1}) profile of the various competitive C−H activation pathways for the benzyl-substituted species **1a**: (a) formation of the C(sp^3)−H activation product; (b) formation of the C(sp^2)−H activation product.

(2.536 Å), a slightly longer C···H distance (1.332 Å), and a shorter O···H bond (1.280 Å).

In order to understand the origin of these differences, a natural bond orbital (NBO) analysis of the electronic structure of the various TSs has been carried out. The NBO analysis yielded Lewis-like structures for all of the transition states that were essentially Ir(III) d^6 complexes with three nonbonding d orbitals at iridium (LP(Ir): lone pairs) and three σ-bonds in a pseudo-fac geometry (Ir−O, Ir−C(carbene), and Ir−C(Cp*)) with three L-type ligands in pseudo-trans positions with respect to the three σ bonds to Ir: two C═C double bonds on Cp* trans to Ir−O and Ir−C(carbene) and the breaking C−H bond trans to Ir−C(Cp*). The various transition states do not correspond to Lewis structures with perfectly localized pairs of electrons occupying either a two-center bond or a one-center lone pair. The departure from this ideally localized picture gives information on the nature of the transformation associated with a given TS. This is particularly illustrative when the natural localized molecular orbitals (NLMO) are considered, as the latter are strictly occupied by two electrons. Therefore, direct comparison between various systems is straightforward as the NLMOs, in contrast to the NBOs, are equally populated in each complex.

In the case of C(sp^3)−H bond activation, the main interactions in the TS pertain to the σ(C−H) bond and one lone pair on iridium. The NLMO σ_{nlmo}(C−H) is essentially developed on the parent NBO σ_{nbo}(C−H) and the antibonding orbital associated with the Ir−C(Cp*) bond (σ_{nlmo}(C−H) = 0.883[σ_{nbo}(C−H)] − 0.398[σ^*_{nbo}(Ir−C)]; see Figure S2 in the Supporting Information). One nonbonding d lone pair on Ir is engaged in a back-donation transfer into σ^*_{nbo}(C−H) (LP$_{nlmo}$(Ir) = 0.920[LP$_{nbo}$(Ir)] − 0.336[σ^*_{nbo}(C−H)]; see Figure S2) that results in the creation of a significant Ir−H bonding interaction. Overall the NBO analysis points to a description of the TS for C(sp^3)−H bond activation as an Ir(V) complex resulting from C−H oxidative addition, in agreement with a significantly large activation barrier.

For **TS-5-4-Ph-anti**, corresponding to C(sp^2)−H activation of the phenyl group, the situation is very different. The σ donation from the C−H bond to Ir is weaker than that

DOI: 10.1021/om501197g
Organometallics XXXX, XXX, XXX−XXX

observed in **TS-5-Int-Ph** (σ_{nlmo}(C−H) = 0.924[σ_{nbo}(C−H)] −0.319[σ^*_{nbo}(Ir−C)]; see Figure S2 in the Supporting Information), but in addition, there is also transfer of electron density from the π cloud of the phenyl ring to the metal, as illustrated by the participation of σ^*_{nbo}(Ir−C) in the π(C═C) NLMO (π_{nlmo}(C═C) = 0.898[π_{nbo}(C═C)] − 0.260-[π^*_{nbo}(C═C′)] − 0.241[π_{nbo}(C═C″)] − 0.172[σ^*_{nbo}(Ir−C)]). The NLMO associated with the C═C bond also contains participations of the NBO associated with the π^* orbitals on the ring as a result of delocalization within the aromatic ring. The participation of the π electron in aromatic C−H activation has already been described in the literature.[2a] The main difference observed in **TS-5-4-Ph-anti** concerns the lack of participation of the d lone pairs in any back-donation into σ^*_{nbo}(C−H). This electron transfer is necessary to achieve bond cleavage and is effective through interaction with a lone pair on oxygen (LP_{nlmo}(O) = 0.961[LP_{nbo}(O)] + 0.235-[σ^*_{nbo}(C−H)]; Figure S2), in agreement with the description of the C(sp^2)−H bond cleavage as an AMLA(4) process. The smoother electron reorganization in **TS-5-4-Ph-anti**, maintaining an Ir(III) situation, explains the lower energy of this TS.

Formally, the NBO analysis for **TS-5-2-Ph** yielded a description similar to that obtained for **TS-5-4-Ph-anti**. The σ donation from σ_{nbo}(C−H) to Ir is weaker (σ_{nlmo}(C−H) = 0.936[σ_{nbo}(C−H)] − 0.251[σ^*_{nbo}(Ir−C)]; see Figure S2 in the Supporting Information), but the transfer from oxygen is stronger (LP_{nlmo}(O) = 0.947[LP_{nbo}(O)] + 0.281[σ^*_{nbo}(C−H)]; Figure S2). This difference in behavior originates from two factors. The π electrons on the pyridinium ring are less available to interact with the metal center, as illustrated by the composition of the π(C═C) NLMO (π_{nlmo}(C═C) = 0.862[π_{nbo}(C═C)] +0.440[π^*_{nbo}(C═N)] + 0.254[π_{nbo}(C═C′)] + 0.08[σ^*_{nbo}(Ir−C)]). The electronegative nitrogen polarizes the π-electron density, rendering the pyridinium ring less apt to interact with Ir. Therefore, the σ donation from C−H is weaker and the OH ligand needs to adapt by increasing its participation. Another aspect, difficult to quantify, concerns the steric repulsion between the two methyl groups on the carbene ligand. For both C(sp^2)−H activation TSs, a five-membered ring is formed with the participation of the iridium center. The dihedral angle C−N−C−C is 16.6° in **TS-5-4-Ph-anti**, whereas the dihedral angle C−C−C−C is 28.1° in **TS-5-2-Ph**. Therefore, the steric repulsion between the methyl groups and the lower coordination ability of the aromatic pyridinium ring result in a less favored geometry for C(sp^2)−H bond cleavage in **TS-5-2-Ph** in comparison to **TS-5-4-Ph-anti** and thus a higher energy.

While these calculations hence provide a rationale for the formation of complexes **2b−d** and **4e**, the observed mixture of **2a** and **3a** cannot be explained by a direct competition of C(sp^2)−H vs C(sp^3)−H bond activation. The kinetic preference deduced from the transition state differences ($\Delta\Delta G^{\ddagger}$ = 3.9 kcal mol^{-1} between **TS-5-Int-Bn** and **TS-5-2-Bn**; Table 2) is one of the largest computed for the series here and would indicate exclusive formation of **2a**. Formation of **3a** must therefore originate from an alternative bond activation pathway. Inspired by the cyclometalation observed en route to **4e**, C−H bond activation of the N-bound benzyl substituent was considered. The transition state for the benzylic C(sp^2)−H activation from **5-OH-Bn-syn** was located at $\Delta G^{\ddagger}$ = 26.9 kcal mol^{-1} and is associated with an AMLA(4) process where the coordinated hydroxide abstracts an hydrogen atom, forming a coordinated water ligand in a single step (Figure 3a). After dissociation of water, the product of the cyclometalation, **6-Bn-syn**, is computed to be more stable than **5-OH-Bn-syn** by ΔG = −15.0 kcal mol^{-1} (Figure 3a). From this intermediate **6**, formation of the C(sp^3)−H activation product $\mathbf{3a_{calc}}$ is achieved in a formal transcyclometalation,[22] involving a metal-mediated hydrogen transfer through a sequence of C(sp^3)−H oxidative addition to form an iridium(V) intermediate followed by reductive elimination. Interestingly, this C(sp^3)−H oxidative addition is computed to be much easier ($\Delta G^{\ddagger}$ = 18.4 kcal mol^{-1}) and less endergonic (ΔG = 9.7 kcal mol^{-1}) than that starting from the monodentate triazolylidene complex **5-OH-Bn-syn** ($\Delta G^{\ddagger}$ = 31.3 kcal mol^{-1} and ΔG = 23.0 kcal mol^{-1}; cf. Table 2). This difference indicates a critical influence of the ancillary ligands, and the benzyl ligand favors access to a high-valent Ir(V) more than the hydroxide ligand. Even though **6-Bn-syn** and **3-Bn** have similar energies, coordination of CH_3CN drives the transformation toward $\mathbf{3a_{calc}}$, which is 3.0 kcal mol^{-1} more stable than the analogous complex $\mathbf{6a_{calc}}$**-syn** (Table S1).

Syn/anti isomerization of **5-OH-Bn** involves rotation of the pyridinyl ring from the syn isomer through a transition state ($\Delta G^{\ddagger}$ = 23.3 kcal mol^{-1}) to give the anti isomer at slightly higher energy (ΔG = 1.8 kcal mol^{-1}; cf. Table 2). This isomerization is easier than C−H activation of the benzyl group ($\Delta G^{\ddagger}$ = 26.9 kcal mol^{-1}; Figure 3a). From the anti isomer, the benzyl C(sp^2)−H bond is activated through an AMLA(4) pathway with an activation barrier of $\Delta G^{\ddagger}$ = 23.9 kcal mol^{-1} to give **6-Bn-anti**. This activation energy is lower than the C(sp^2)−H activation of the pyridinium ring ($\Delta G^{\ddagger}$ = 25.6 kcal mol^{-1}; cf. Table 2); however, the kinetic preference is only 1.7 kcal mol^{-1} and hence is significantly weaker for benzyl compared to phenyl C−H bond activation ($\Delta\Delta G^{\ddagger}$ = 6.2 kcal mol^{-1}). This reduced kinetic preference is explained by the increase in the ring size needed to reach the geometry adapted to C(sp^2)−H benzyl activation in **5-OH-Bn-anti** in comparison to that needed in **5-OH-Ph-anti**. The coordination of the π system of the aromatic ring of the benzyl group, needed in the C−H activation process, as previously explained in the case of phenyl, imposes a boatlike six-membered ring in **TS-5-6-AMLA4-Bn-anti** that destabilizes the transition state. This constraint does explain why the C(sp^2)−H activation of the benzyl group is closer in energy to the C(sp^2)−H activation of the pyridinium unit.

After water dissociation, **6-Bn-anti** is computed to be more stable than **5-OH-Bn-anti** by ΔG = −15.1 kcal mol^{-1} (Figure 3b). From this intermediate, C(sp^2)−H activation of the pyridinium group is effective in a two-step oxidative addition reductive elimination process with transition states at $\Delta G^{\ddagger}$ = 18.3 kcal mol^{-1} and $\Delta G^{\ddagger}$ = 7.0 kcal mol^{-1}, respectively, to afford **2-Bn** (Figure 3b). Interestingly, these calculations suggest a similar activation barrier for C(sp^2)−H oxidative addition from **6-Bn-anti** and C(sp^3)−H oxidative addition from **6-Bn-syn**. In addition, formation of **2-Bn** from **6-Bn-anti** is endergonic with ΔG = 6.8 kcal mol^{-1} and coordination of acetonitrile does not reverse the stability order, as $\mathbf{6a_{calc}}$**-anti** is computed to be more stable than $\mathbf{2a_{calc}}$ by ΔG = 1.3 kcal mol^{-1} (Table S1 in the Supporting Information).

There are thus two apparently disconnected pathways forming **2a** and **3a**. The computed data in Figure 3 indicate that C−H activation of the benzyl group is preferred from the anti rather than the syn isomer by $\Delta\Delta G^{\ddagger}$ = 1.2 kcal mol^{-1}. As the isomerization between **5-OH-Bn-syn** and **5-OH-Bn-anti** is easier than the two C−H activation processes, the $\Delta\Delta G^{\ddagger}$ value

DOI: 10.1021/om501197g
Organometallics XXXX, XXX, XXX−XXX

is relevant for selectivity and translates into an 85% to 15% preference to follow the pathway leading to $\mathbf{2a}_{calc}$ vs $\mathbf{3a}_{calc}$. However, if acetonitrile coordination is assumed to be faster than the processes interconverting the various species in Figure 3, the final ratio of the observed products is dictated by the kinetic preference. The transition state interconverting **6-Bn-anti** to **6-Bn-syn** through rotation of the pyridine ring has been located at $\Delta G^{\ddagger}$ = 20.9 kcal mol^{-1} above **6-Bn-anti** (Table S1 in the Supporting Information). Therefore, the pathway leading from **6-Bn-anti** to **2-Bn** is favored by $\Delta\Delta G^{\ddagger}$ = 1 kcal mol^{-1} over the trajectory leading to **6-Bn-syn**; the initial kinetic partition between the two pathways is expected to be preserved among the various acetonitrile adducts. Hence, the reaction mixture should consist of $\mathbf{2a}_{calc}$ (12%), $\mathbf{3a}_{calc}$ (15%), and a mixture of syn and anti isomers of $\mathbf{6a}_{calc}$ (73%). This ratio is in excellent agreement with the experimental observations (see above).

Upon longer reaction times, the isomerization between the syn and the anti configuration of **6-Bn** offers a pathway to switch from one route to the other. Under thermodynamic reaction control, this isomerization is predicted to lead to the exclusive formation of $\mathbf{3a}_{calc}$. However, acetonitrile has to dissociate before any reaction is possible. Modeling kinetic behavior when solvent dissociation is implicated is a difficult task. One crude way to estimate the rate of reaction involving solvent dissociation is to approximate the activation barrier to the binding enthalpy of the solvent: $\Delta G^{\ddagger} = \Delta H$. The acetonitrile binding enthalpies to **3-Bn**, **6-Bn-syn**, and **6-Bn-anti** have similar values (17.9, 15.8, and 17.5 kcal mol^{-1}, respectively). These values indicate that the three corresponding acetonitrile complexes should eventually be distributed according to their respective energy, independently of the kinetic distribution observed in the crude mixture. Therefore, only $\mathbf{3a}_{calc}$ should be observed at long reaction times. Acetonitrile binding to **2-Bn** is significantly stronger (ΔH = 22.5 kcal mol^{-1}), therefore implying that the reverse reaction, i.e. dissociation of CH_3CN from $\mathbf{2a}_{calc}$ to **2-Bn** in order to form **6-Bn-anti**, is more difficult. Consequently, the initial kinetic proportion of $\mathbf{2a}_{calc}$ will remain constant in the final thermodynamic distribution. Once the thermodynamic equilibrium has been reached, the final mixture should be composed of **3a** and **2a** in a relative ratio of approximately 9:1, a ratio that matches the experimental data very well (see above).

These calculations for **1a** indicate that the C−H activation of the benzyl ring is kinetically preferred over C(sp^2)−H or C(sp^3)−H activation of the pyridinium unit. Two benzyl C−H activation processes are competitive, according to the relative orientation of the pyridinium heterocycle with respect to the hydroxyl ligand. The two benzyl-metalated intermediates $\mathbf{6a}_{calc}$ resulting from these C−H activation processes constitute the major species in the crude reaction mixture. These cyclometalated intermediates undergo a trans-cyclometalation reaction,[22] forming either $\mathbf{2a}_{calc}$ or $\mathbf{3a}_{calc}$. The metalated benzyl group significantly reduces the activation barriers associated with C(sp^3)−H activation to such an extent that it becomes competitive with the C(sp^2)−H activation of the pyridinium unit. Therefore, the final product becomes the thermodynamically more favored complex **3** and not the kinetically preferred pyridylidene complex **2** as observed with **1b−d** that lack the possibility to metalate the N-bound substituents.

Reactions at Room Temperature. Relevant intermediates of this C(sp^3)−H bond activation process were experimentally detected upon altering the reaction conditions. When the reaction was carried at room temperature rather than at 80 °C, the monodentate complex **5a** was isolated (Scheme 3). This

Scheme 3. Formation of the Monodentate Complex 5a

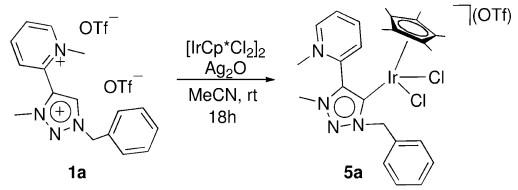

complex was characterized spectroscopically, and the iridium-bound carbene carbon resonates at δ_C 145.1 ppm, in agreement with related monodentate triazolylidene iridium(III) complexes.[14] Rotation about the N−C_{Bn} bond is hindered upon metalation; thus, the benzylic CH_2 protons appear as AB doublets ($^2J_{HH}$ = 15.7 Hz). When this complex was heated in the presence of Ag_2O, activity was observed identical with that on starting from the corresponding triazolium salt **1a**, thus confirming the role of this monodentate triazolylidene species as a most likely intermediate for the second C−H bond activation process and validating the starting points used for the computational studies (cf. **5-OH-R** in Figures 2 and 3). It should be noted that the Cp* resonance frequency of this monodentate species does not correspond to that of the intermediates observed in the crude reaction mixtures for the second C−H activation (see above). Consequently, we assume that the intermediates apparent in the final crude mixture are products of subsequent steps such as the computationally predicted benzyl C(sp^2)−H activation.

Upon standing or slight heating, complex **5a** gradually undergoes benzylic C(sp^2)−H bond activation and affords complex **6a** (Scheme 4). This cyclometalation step was significantly accelerated in the presence of OAc^-, a concept common to aryl C−H bond activation by iridium(III) centers.[23] However, the cyclometalated complex **6a** lacks stability in the solid state and gradually and spontaneously reacts to give the corresponding trans-cyclometalated complex **3a** (Scheme 4). This instability prevented full analyses of complex **6a**, though it was characterized in solution. Two Cp* resonances are observed in the ^{1}H NMR spectra of **6a** in about a 2:1 ratio (δ_H 1.56 and 1.50 ppm), which have been attributed to well-resolved rotamers featuring the pyridine-bound methyl group either syn or anti to the iridium center. Nuclear Overhauser effect (NOE) experiments on **6a** indicate that the syn complex is the major rotamer.[24] Iridium coordination to the benzylic unit is implied by the loss of one phenyl proton in both rotamers, and the phenyl group featured four inequivalent signals in the aromatic region, indicating desymmetrization of the phenyl group due to cyclometalation (cf. **4e**). A diagnostic feature for cyclometalation is the upfield shift of the benzylic CH_2 resonances and the larger signal separation for all species in comparison to the AB doublet in **5**. The well-resolved AX signal in **6** is presumably a result of the steric hindrance imposed by the newly formed metallacycle. The doublet signals are well resolved for the two rotamers of **6a** at δ_H 5.62 and 5.05 pm (^2J = 14.8 Hz; syn isomer) and δ_H 5.63 and 5.09 ppm (^2J = 15.2 Hz; anti isomer). The carbene carbons of **6a** appear at essentially identical frequencies for both rotamers (δ_C 140.8 ppm), and also the iridium-bound benzyl carbons are barely distinguishable (δ_C 140.0 ppm), in agreement with related complexes.[14,21] The spectral data of complex **6a** are identical

DOI: 10.1021/om501197g
Organometallics XXXX, XXX, XXX−XXX

Scheme 4. Synthesis of the Benzyl CH Activated Complex 6a Followed by Conversion to the Ylide Complex 3a

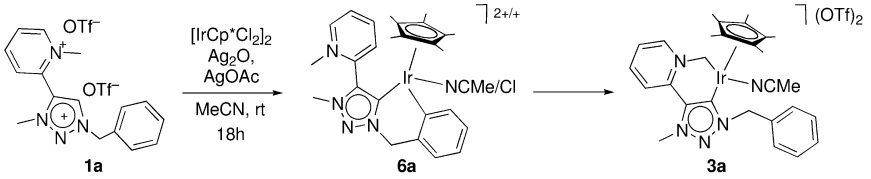

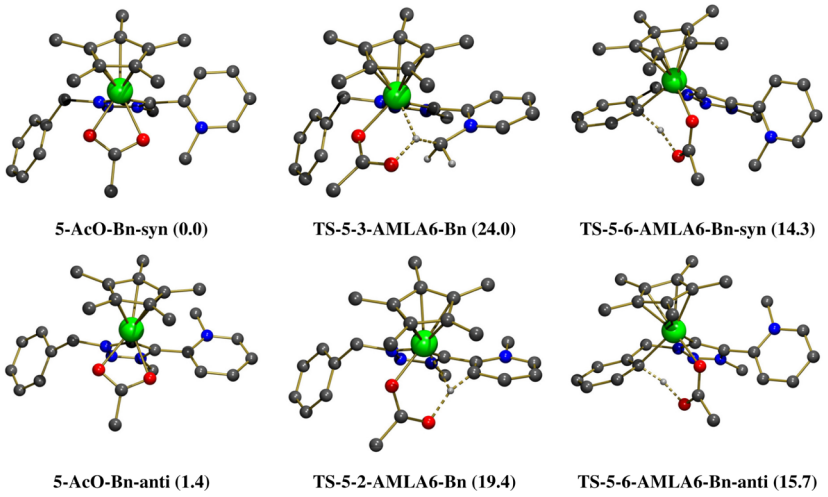

Figure 4. Geometry and Gibbs energy (298 K, kcal mol^{-1}, relative to **5-AcO-Bn-syn**) of the κ^2-AcO precursors and the TS corresponding to the various C−H activation processes (most H atoms omitted for clarity).

with those of the intermediates observed in the crude reaction mixture (see above).

Upon heating in MeCN solution, the cyclometalated intermediate **6a** transformed exclusively to the C(sp^3)−H bond activated complex **3a**, and no formation of the C(sp^2)-metalated dicarbene complex **2a** was detected from **6**. This observation is in excellent agreement with the calculated trajectory (cf. Figure 3), which predicted syn/anti isomerization of complex **6** and also similar barriers for the C(sp^3)−H and C(sp^2)−H activation toward **3** and **2** yet a significant thermodynamic preference to form **3** (9:1 vs **2**).

The addition of acetate promoted the sequential transformation from **5** to **6** and subsequently to **3** at room temperature. Coordination of acetate to iridium opens the possibility to induce C−H activation through a comparably easy AMLA(6) pathway.[20] Accordingly, the κ^2-OAc complexes **5-AcO-Bn-syn** and **5-AcO-Bn-anti** were the computed precursors of the subsequent C−H activation processes (Figure 4). C(sp^3)−H and C(sp^2)−H activations of the pyridine ring are computed to be much easier than those with coordinated hydroxide (activation barriers at 298 K as low as $\Delta G^{\ddagger}$ = 24.0 and 18.0 kcal mol^{-1}, respectively; Figure 4). In the transition state between **5** and **3a**$_{calc}$, the C(sp^3)−H bond is significantly elongated (1.33 Å), the Ir···C(sp^3) bond is still long at 2.47 Å, and the O···H bond is not yet formed (1.50 Å). Even still the relative energy of this transition state with respect to **5-AcO-Bn-syn** is not too high. Typical for an AMLA(6) process, the hydrogen transfer from C to O is achieved in one step, even from the C(sp^3) site. However, the acetate does not reverse the kinetic preference for C(sp^2)−H over C(sp^3)−H activation of the pyridinium unit and C(sp^2)−H activation of the benzyl ring is computed to be much easier with $\Delta G^{\ddagger}$ = 14.3 kcal mol^{-1} from either the syn or the anti isomer of **5-AcO-Bn** (Figure 4).

The chelate complexes resulting from benzyl C−H activation and dissociation of AcOH, **6-Bn-syn** and **6-Bn-anti**, are both more stable than the κ^2-OAc precursor **5-AcO-Bn-syn** by ΔG = −3.6 and −1.8 kcal mol^{-1}, respectively. Coordination of acetonitrile stabilizes the complexes even further with ΔG = −8.3 and −6.7 kcal mol^{-1} with respect to **5-AcO-Bn-syn**, respectively. In agreement with the experimental observations, the syn rotamer is more stable than the anti species. At room temperature, reaction of **6a**$_{calc}$**-anti** to form **2a**$_{calc}$ involves an activation barrier of $\Delta G^{\ddagger}$ = 24.0 kcal mol^{-1} and is endergonic by ΔG = 1.5 kcal mol^{-1}. Isomerization to **6a**$_{calc}$**-syn** is less demanding ($\Delta G^{\ddagger}$ = 20.9 kcal mol^{-1}) and exergonic (ΔG = −1.6 kcal mol^{-1}). Reaction of the syn isomer to form **3a**$_{calc}$ passes through an activation barrier of $\Delta G^{\ddagger}$ = 21.5 kcal mol^{-1} at room temperature and is exergonic with ΔG = −3.5 kcal mol^{-1}. These data thus indicate that syn/anti isomerization of **6a**$_{calc}$ is faster than disappearance of both complexes to form either **3a**$_{calc}$ or **2a**$_{calc}$. Moreover, formation of **2a**$_{calc}$ is not preferred kinetically or thermodynamically, in agreement with the exclusive observation of **3a** experimentally in the presence of acetate. Moreover, the syn/anti isomers of intermediate **6a** are sufficiently long-lived to be observed experimentally at room temperature (cf. the discussion above).

Kinetic Analyses. Switching the solvent from MeCN to methanol or CH_2Cl_2 substantially accelerated the trans-cyclometalation process, pointing to a critical role of MeCN dissociation from the cyclometalated intermediate **6a** to induce the bond activation process, as predicted computationally. Performing the reaction in CD_3OD allowed the C(sp^3)−H bond activation process from complex **6a** to be monitored by solution NMR spectroscopy, which revealed that consumption of **6a** was accompanied by concomitant and exclusive formation of **3a**. Moreover, deuterium labeling of the two N-bound methyl groups of **1a** afforded the hexadeuterated complex **3a**-

DOI: 10.1021/om501197g
Organometallics XXXX, XXX, XXX−XXX

D_6, which features selective D incorporation into the ortho position of the benzylic group. This reactivity pattern further validates the relevance of intermediate **6a** and subsequent hydrogen transfer in a trans-cyclometalation reaction. Strong support for a fully intramolecular hydrogen transfer was provided by an experiment starting from a 1:1 mixture of **1a-D_6** and nondeuterated **1a**, which afforded only **3a-D_6** and undeuterated **3a** according to mass spectrometric analyses ([M − OTf]$^+$ signals at m/z 780.76 and 786.83). Intermolecular crossover of a hydrogen/deuterium upon (trans)-cyclometalation would lead to **3a-D_5**, but this isotope was not detected even in traces.[16]

Time-dependent monitoring of the hydrogen transfer from the pyridinium site to the cyclometalated benzyl unit gave access to the relevant rate constants for the transformation of **6a** to **3a** (Table 3). The reaction is first order in iridium (Figure S3 in the Supporting Information), hence supporting an intramolecular hydrogen migration. When ligand precursor **1a-D_6** is used with N-bound CD_3 groups, the trans-cyclometalation rate is substantially lower than that with the undeuterated system and the kinetic isotope effect is large: KIE = 9.3 at 328 K. This result supports C−H/D bond cleavage as the rate-determining step, as suggested by the calculated maxima in Figure 3. Rate constants were determined at different temperatures to further elucidate the rate-determining step (Table 3). The corresponding Eyring plot was linear (Figure S4 in the Supporting Information) and yielded the pertinent enthalpy and entropy of activation for the trans-cyclometalation: i.e., the transformation of **6a** to **3a** ($\Delta H^{\ddagger}$ = 33.2 ± 1.7 kcal mol^{-1} and $\Delta S^{\ddagger}$ = 23.0 ± 4.8 cal mol^{-1} K^{-1}). The slightly positive entropy of activation aligns well with the release of MeCN as ancillary ligand and with the higher order in the computed transition state (cf. Figure 3) and may also be associated with the loss of syn/anti isomerization of the methylpyridinium unit.

Table 3. Observed First-Order Rate Constants of Transcyclometalation To Transform 6a to 3a

complex	T/K	$k_{obs}/10^{-6}$ s^{-1}
6a	328	74.2 ± 0.9
6a-D_6	328	8.5 ± 0.4
6a	308	1.3 ± 0.01
6a	313	6.6 ± 0.06
6a	318	8.6 ± 0.01
6a	323	27.6 ± 0.14
6a	328	74.2 ± 3.93
6a	338	183.7 ± 5.0

Computation of the methanol complexes **6-MeOH-Bn** revealed the anti conformer to be more stable than the syn analogue by ΔG = 1.3 kcal mol^{-1} (smd in methanol at 298 K), though MeOH dissociation inverts this order and the syn isomer is more stable by ΔG = −1.8 kcal mol^{-1}. As expected, dissociation of methanol is easier than dissociation of MeCN, with ΔE = 9.6 and 13.2 kcal mol^{-1} for the syn and anti isomers, respectively (cf. ΔE = 17.6 and 19.4 kcal mol^{-1}, respectively, for the corresponding MeCN dissociation process). There is thus an energy penalty of ca. 6−8 kcal mol^{-1} when using acetonitrile as a solvent. The energy of the rate-determining transition state along the pathway to **3a** reveals a calculated value of $\Delta E^{\ddagger}$ = 27.4 kcal mol^{-1}, in good agreement with the experimentally determined $\Delta H^{\ddagger}$ value. These data further validate the dual experimental and theoretical approach to detail the pathway of this remarkable C(sp^3)−H bond activation process.

CONCLUSIONS

Using iterative experimental and computational methods, we have determined the mechanistic pathway for both pyridinium C(sp^2)−H activation and C(sp^3)−H activation occurring at a triazolylidene iridium(III) scaffold. Specifically, this combined approach elucidated the remarkable correlation between the site of bond activation and the remote benzyl substituents on the triazolylidene. Accordingly, also in the C(sp^3)−H bond activation process, initial cleavage of an aryl C−H bond is preferred over alkyl C−H bond activation, regardless of the N-bound wingtip group. However, if the N-bound substituent is a phenyl or benzyl group, C_{aryl}−H bond activation is preferred over $C_{pyridinium}$−H bond cleavage. This cyclometalated species is stable for phenyl substituents but not for benzyl substituents and provides a suitable configuration for subsequent trans-cyclometalation via C(sp^3)−H activation of the N-bound methyl group. These results further suggest that the C−H bond activation reactivity of the benzyl group is key to influence the selectivity of the C−H bond activation processes at the remote pyridine ring, as the latter proceeds through the intermediacy of a cyclometalated species. Opportunities to influence the selectivity of the C−H bond activation process hence become available, since aryl C−H activation by electrophilic transition metals is well understood.[25]

Experimental and computational work is in alignment with this C(sp^3)−H activation to proceed via an oxidative addition/reductive elimination sequence. Elucidation of the intimate steps of these intramolecular C−H bond activations will be critical for designing efficient intermolecular and eventually catalytic processes for iridium-mediated C(sp^3)−H functionalization also using more general substrates.

EXPERIMENTAL SECTION

General Considerations. The syntheses of the iridium complexes were carried out under an inert atmosphere of N_2 using Schlenk techniques and dry solvents. Purifications were performed in air using commercial solvents. ^{1}H and ^{13}C{^{1}H} NMR spectra were recorded at room temperature on Varian spectrometers operating at 400 or 500 MHz unless stated otherwise. Chemical shifts (δ in ppm, J in Hz) were referenced to $SiMe_4$. Signal assignments are based on homo- and heteronuclear (multiple-bond) correlation spectroscopy. Elemental analyses were performed by the Microanalytical Laboratory at the University College Dublin, Ireland. High-resolution mass spectrometry was carried out with a Micromass/Waters Corp. USA liquid chromatography time-of-flight spectrometer equipped with an electrospray source. The precursors $[Cp^*IrCl_2]_2$[26] and **1a**[11] and complexes **2a,b**, **3a**, and **4e** were prepared according to literature procedures.[11,12] The previously reported azide precursor 2-phenylethyl azide[27] was prepared according to a modified procedure.[16] All other reagents were purchased from commercial sources and were used as received, unless otherwise stated. Room temperature is 18 °C unless otherwise stated.

Compound 1c. 1-(Pentafluorobenzyl)-4-(2-pyridyl)-1,2,3-triazole[16] (0.30 g, 0.92 mmol) and MeOTf (0.60 g, 3.6 mmol) were refluxed in CH_2Cl_2 (8 mL) for 16 h. A white precipitate formed during this time, which was collected and washed with CH_2Cl_2 (5 × 5 mL) and with Et_2O (5 × 10 mL), and dried in vacuo to afford **6** as a white solid (580 mg, 96%). ^{1}H NMR (DMSO-d_6, 500 MHz): δ 9.47 (s, 1H, H_{trz}), 9.39 (d, $^3J_{HH}$ = 6.0 Hz, 1H, H_{py}^6), 8.87 (t, $^3J_{HH}$ = 7.5 Hz, 1H, H_{py}^4), 8.45 (ddd, $^3J_{HH}$ = 7.5 Hz, $^3J_{HH}$ = 6.0 Hz, $^4J_{HH}$ = 1.0 Hz, 1H, H_{py}^5), 8.43 (dd, $^3J_{HH}$ = 7.5 Hz, $^4J_{HH}$ = 1.0 Hz, 1H, H_{py}^3), 6.25 (s, 2H, CH_2), 4.28 (s, 3H, $N_{trz}CH_3$), 4.27 (s, 3H, $N_{py}CH_3$). ^{13}C{^{1}H} NMR (CD_3CN, 125 MHz): δ 149.6 (C_{py}^6), 146.9 (C_{py}^4), 137.2 (C_{py}^2), 134.3

DOI: 10.1021/om501197g
Organometallics XXXX, XXX, XXX−XXX

(C_{trz}–H), 133.1 (C_{trz}–py), 132.2 (C_{py}^{3}), 130.9 (C_{py}^{5}), 121.0 (q, $^{1}J_{CF}$ = 322 Hz, CF_3SO_3), 47.9 ($N_{py}CH_3$), 44.9 (NCH_2Ar_F), 40.0 ($N_{trz}CH_3$). ^{19}F NMR (CD_3CN, 282 MHz): δ −77.8 (s), −140.0 (m), −151.0 (m), −161.6 (m). Anal. Calcd for $C_{18}H_{13}F_{11}N_4O_6S_2$ (654.43): C, 33.04; H, 2.00; N, 8.56. Found: C, 32.62; H, 1.88; N, 8.47.

Compound 1d. 1-(2-Phenylethyl)-4-(2-pyridyl)-1,2,3-triazole[16] (205 mg, 0.82 mmol) and MeOTf (0.54 g, 3.3 mmol) were refluxed in CH_2Cl_2 (8 mL) for 16 h. A white precipitate formed during this time, which was collected and washed with CH_2Cl_2 (2 × 5 mL) and with Et_2O (5 × 10 mL), and dried in vacuo to afford **1d** as a white solid (455 mg, 96%). ^{1}H NMR (CD_3CN, 500 MHz): δ 9.04 (d, $^{3}J_{HH}$ = 6.0 Hz, 1H, H_{py}^{6}), 8.87 (t, $^{3}J_{HH}$ = 7.8 Hz, 1H, H_{py}^{4}), 8.74 (s, 1H, H_{trz}), 8.32 (dd, $^{3}J_{HH}$ = 7.8 Hz, $^{3}J_{HH}$ = 6.0 Hz, 1H, H_{py}^{5}), 8.43 (d, $^{3}J_{HH}$ = 7.8 Hz, 1H, H_{py}^{3}), 7.42–7.33 (m, 5H, H_{Ph}), 4.99 (t, $^{3}J_{HH}$ = 7.4 Hz, 2H, CH_2–trz), 4.23 (s, 3H, $N_{trz}CH_3$), 4.17 (s, 3H, $N_{py}CH_3$), 3.41 (t, $^{3}J_{HH}$ = 7.4 Hz, 2H, CH_2-Ph). ^{13}C{^{1}H} NMR (CD_3CN, 125 MHz): δ 149.7 (C_{py}^{6}), 147.3 (C_{py}^{4}), 136.9 (C_{py}^{2}), 136.0 (C_{Ph}-alkyl), 133.1 (C_{trz}-H), 132.6 (C_{trz}-py), 132.5 (C_{py}^{3}), 131.2 (C_{py}^{5}), 129.2, 129.1, 127.6 (3 × C_{Ph}-H), 55.8 (CH_2-trz), 47.8 ($N_{py}CH_3$), 39.6 ($N_{trz}CH_3$), 35.0 (CH_2-Ph). Anal. Calcd for $C_{19}H_{20}F_6N_4O_6S_2$ (578.07): C, 39.45; H, 3.48; N, 9.68. Found: C, 32.62; H, 1.88; N, 8.47.

Complex 2c. A mixture of **1c** (100 mg, 0.15 mmol), Ag_2O (36 mg, 0.15 mmol), and $[Cp^*IrCl_2]_2$ (61 mg, 0.08 mmol) was refluxed in dry MeCN (15 mL) for 20 h. The reaction was filtered through Celite, and all volatiles were removed under reduced pressure. The residue was purified by gradient column chromatography (SiO_2; CH_2Cl_2 then CH_2Cl_2/MeCN 5/2 v/v), thus yielding complex **4** as a yellow solid (55 mg, 36%). ^{1}H NMR (CD_3CN, 400 MHz): δ 8.70 (dd, $^{3}J_{HH}$ = 7.7 Hz, $^{4}J_{HH}$ = 0.9 Hz, 1H, H_{py}^{4}), 8.30 (dd, $^{3}J_{HH}$ = 6.1 Hz, $^{4}J_{HH}$ = 0.9 Hz, 1H, H_{py}^{6}), 7.52 (dd, $^{3}J_{HH}$ = 6.1 Hz, $^{3}J_{HH}$ = 7.7 Hz, 1H, H_{py}^{5}), 5.94, 5.76 (2 × d, $^{2}J_{HH}$ = 14.6 Hz, 1H, $CH_2C_6F_5$), 4.56 (s, 3H, $N_{py}CH_3$), 4.52 (s, 3H, $N_{trz}CH_3$), 1.86 (s, 15H, Cp-CH_3). ^{13}C{^{1}H} NMR (CD_3CN, 100 MHz): δ 155.4 (C_{trz}-Ir), 154.0 (C_{py}-Ir), 153.0 (C_{py}^{4}), 152.6 (C_{py}^{3}), 149.1 (C_{trz}-py), 140.3 (C_{py}^{6}), 125.5 (C_{py}^{5}), 94.8 (C_{Cp}-Me), 49.8 ($N_{py}CH_3$), 44.7 ($N_{trz}CH_2Ar_F$), 44.4 ($N_{trz}CH_3$), 9.0 (Cp-CH_3). ^{19}F NMR ($CDCl_3$, 376.3 MHz): δ −79.4 (s), −142.1 (m), −153.5 (m), −163.3 (m). Anal. Calcd for $C_{30}H_{29}F_{11}IrN_5O_6S_2$ (1020.9): C, 35.29; H, 2.86; N, 6.86. Found: C, 35.08; H, 2.68; N, 6.79.

Complex 2d. A mixture of **1d** (300 mg, 0.52 mmol), Ag_2O (119 mg, 0.52 mg), and $[Cp^*IrCl_2]_2$ (206 mg, 0.26 mmol) was refluxed in dry MeCN (10 mL) for 18 h. The reaction mixture was filtered through Celite, and all volatiles were removed under reduced pressure. The residue was purified by gradient column chromatography (SiO_2; CH_2Cl_2 then CH_2Cl_2/MeCN 1/1 v/v), thus yielding complex **2d** as a yellow solid. By NMR spectroscopy, a second product (approximately 25%) was observed that featured slightly shifted pyridylidene protons, only four aryl protons, and a distinctly high field shifted NCH_3 group at δ 4.00. This impurity was tentatively assigned to a doubly cyclometalated species. Further attempts to separate the two species have been unsuccessful thus far, and only spectroscopic data for **2d** are therefore reported. ^{1}H NMR (CD_3CN, 500 MHz): δ 8.70 (d, $^{3}J_{HH}$ = 7.7 Hz, 1H, H_{py}^{4}), 8.30 (d, $^{3}J_{HH}$ = 6.1 Hz, 1H, H_{py}^{6}), 7.52 (dd, $^{3}J_{HH}$ = 6.1 Hz, $^{3}J_{HH}$ = 7.7 Hz, 1H, H_{py}^{5}), 7.40–7.25 (m, 5H, H_{Ph}), 4.91, 4.80 (2 × dt, $^{2}J_{HH}$ = 13.5 Hz, $^{3}J_{HH}$ = 7.3 Hz, 1H, CH_2-trz), 4.58, 4.57 (2 × s, 3H, NCH_3), 3.39 (t, $^{3}J_{HH}$ = 7.3 Hz, 2H, CH_2-Ph), 1.81 (s, 15H, Cp-CH_3). ^{13}C{^{1}H} NMR (CD_3CN, 125 MHz): δ 154.1 (C_{py}-Ir), 153.7 (C_{trz}-Ir), 152.4 (C_{py}^{4}), 148.8 (C_{py}^{5}), 140.0 (C_{py}^{6}), 137.0 (C_{Ph}-alkyl), 129.0, 128.9, 127.3 (3 × C_{Ph}-H), 125.2 (C_{py}^{2}), 94.3 (Cp*), 54.7 (CH_2–trz), 49.7 ($N_{py}CH_2$), 44.1 ($N_{trz}CH_3$), 35.3 (CH_2-Ph), 8.8 (Cp-CH_3), C_{trz}-py not detected.

Complex 5a. Compound **1a** (0.206 g, 0.37 mmol), Ag_2O (0.110 g, 0.47 mmol), and $[IrCp^*Cl_2]_2$ (0.146 g, 0.18 mmol) were stirred for 18 h in MeCN (10 mL) under the exclusion of light. The reaction mixture was filtered through Celite, and the filtrate was concentrated to 2 mL. After addition of Et_2O (50 mL), **6a** was isolated as a yellow solid (yield 0.172 g, 58%). ^{1}H NMR (400 MHz, CD_2Cl_2): δ 8.95 (d, $^{3}J_{HH}$ = 6.0 Hz, 1H, H_{py}^{6}), 8.62 (t, $^{3}J_{HH}$ = 7.8 Hz, 1H, H_{py}^{4}), 8.35 (d, $^{3}J_{HH}$ = 7.8 Hz, 1H, H_{py}^{3}), 8.15 (dd, $^{3}J_{HH}$ = 6.0 Hz, 7.8 Hz, 1H, H_{py}^{5}), 7.48 (t, $^{3}J_{HH}$ = 7.4 Hz, 2H, H_{Ph}^{meta}), 7.39 (t, $^{3}J_{HH}$ = 7.4 Hz, 1H, H_{Ph}^{para}), 7.30 (d, $^{3}J_{HH}$ = 7.4 Hz, 1H, H_{Ph}^{ortho}), 5.89, 5.79 (AB doublet, $^{2}J_{HH}$ = 15.6 Hz, 2H, CH_2), 4.23 (s, 3H, N_{py}–CH_3), 4.01 (s, 3H, N_{trz}–CH_3), 1.61 (s, 15H, $Cp(CH_3)_5$). ^{13}C{^{1}H} NMR (101 MHz, CD_2Cl_2): δ 148.4 (C_{py}^{6}), 146.2 (C_{py}^{4}), 145.1 (C_{trz}-Ir), 142.9 (C_{py}^{2}), 138.9 (C_{trz}-py), 134.7 (C_{Ph}-CH_2), 133.6 (C_{py}^{3}), 130.2 (C_{py}^{5}), 129.7 (C_{Ph}^{meta}), 129.1 (C_{Ph}^{para}), 127.4 (C_{Ph}^{ortho}), 121.1 (q, $^{1}J_{CF}$ = 320.4 Hz, SCF_3) 92.5 (Cp), 57.8 (CH_2), 49.2 (N_{py}-CH_3), 39.1 (N_{trz}-CH_3), 9.3 ($Cp(CH_3)_5$). MS: m/z 777.1442 $[M - Cl]^+$, calculated for $C_{28}H_{33}ClF_3IrN_3O_3S$ 777.1465.

Complex 6a. Compound **1a** (0.100 g, 0.18 mmol), Ag_2O (0.043 g, 0.18 mmol), AgOAc (0.043 g, 0.27 mmol), and $[IrCp^*Cl_2]_2$ (0.071 g, 0.09 mmol) were stirred in MeCN (10 mL) for 18 h at room temperature under the exclusion of light. The reaction mixture was filtered through Celite, and the filtrate was dried in vacuo (major rotamer/minor rotamer 2/1). The complex was stored in acetonitrile solution, and the yield was determined to be quantitative by NMR spectroscopy. Data for the major rotamer (**syn-6a**) are as follows. ^{1}H NMR (400 MHz, CD_3CN): δ 9.08 (d, $^{3}J_{HH}$ = 6.1 Hz, 1H, H_{py}^{6}), 8.87 (t, $^{3}J_{HH}$ = 8.9 Hz, 1H, H_{py}^{4}), 8.37–8.30 (m, 2H, H_{py}^{3} and H_{py}^{5}), 7.41 (d, $^{3}J_{HH}$ = 7.5 Hz, 1H, $H_{Ph}^{ortho\ Ir}$), 7.26 (d, $^{3}J_{HH}$ = 7.5 Hz, 1H, $H_{Ph}^{ortho\ CH_2}$), 7.08–6.97 ($H_{Ph}^{meta\ Ir}$ and $H_{Ph}^{meta\ CH_2}$), 5.62 (d, $^{2}J_{HH}$ = 14.8 Hz, 1H, CH_2), 5.05 (d, $^{3}J_{HH}$ = 14.8 Hz, 1H, CH_2), 3.97 (s, 3H, N_{trz}-CH_3), 3.89 (s, 3H, N_{py}-CH_3), 1.56 (s, 15H, $Cp(CH_3)_5$). ^{13}C{^{1}H} NMR (101 MHz, CD_3CN): δ 150.5 (C_{py}^{6}), 148.2 (C_{py}^{4}), 140.8 (C_{trz}–Ir), 140.7 ($C_{Ph}^{ortho\ Ir}$), 140.0 (C_{Ph}-Ir), 138.8 (C_{Ph}-CH_2), 138.3 (C_{trz}-py), 134.7 (C_{py}^{3}), 131.9 (C_{py}^{5}), 129.5 ($C_{Ph}^{meta\ Ir}$), 127.3 ($C_{Ph}^{ortho\ CH_2}$), 124.7 ($C_{Ph}^{meta\ CH_2}$), 93.9 (Cp), 60.3 (CH_2), 48.0 (N_{py} CH_3), 39.3 (N_{trz} CH_3), 9.6 ($Cp(CH_3)_5$), C_{py}^{2} not resolved. Data for the minor rotamer (**anti-6a**) are as follows. ^{1}H NMR (400 MHz, CD_3CN): δ 9.10 (d, $^{3}J_{HH}$ = 6.1 Hz, 1H, H_{py}^{6}), 8.76 (t, $^{3}J_{HH}$ = 8.0 Hz, 1H, H_{py}^{4}), 8.37–8.30 (m, 1H, H_{py}^{5}), 8.05 (d, $^{3}J_{HH}$ = 8.0 Hz, 1H, H_{py}^{3}), 7.44 (d, $^{3}J_{HH}$ = 7.4 Hz, 1H, $H_{Ph}^{ortho\ Ir}$), 7.26 (d, $^{3}J_{HH}$ = 7.4 Hz, 1H, $H_{Ph}^{ortho\ CH_2}$), 7.08–6.97 ($H_{Ph}^{meta\ Ir}$ and $H_{Ph}^{meta\ CH_2}$), 5.63 (d, $^{2}J_{HH}$ = 15.2 Hz, 1H, CH_2), 5.09 (d, $^{2}J_{HH}$ = 15.2 Hz, 1H, CH_2), 4.34 (s, 3H, N_{py}-CH_3), 3.99 (s, 3H, N_{trz}-CH_3), 1.52 (s, 15H, $Cp(CH_3)_5$). ^{13}C{^{1}H} NMR (101 MHz, CD_3CN): δ 150.2 (C_{py}^{6}), 147.7 (C_{py}^{4}), 140.8 (C_{trz}–Ir), 140.5 ($C_{Ph}^{ortho\ Ir}$), 140.0 (C_{Ph}-Ir), 138.8 (C_{Ph}-CH_2), 134.4 (C_{py}^{3}), 131.4 (C_{py}^{5}), 129.6 ($C_{Ph}^{meta\ Ir}$), 127.2 ($C_{Ph}^{ortho\ CH_2}$), 124.7 ($C_{Ph}^{meta\ CH_2}$), 93.8 (Cp), 60.4 (CH_2), 47.9 (N_{py}-CH_3), 39.3 (N_{trz}-CH_3), 9.5 ($Cp(CH_3)_5$), C_{py}^{2} and C_{trz}-py not resolved.

Kinetic Measurements. The starting concentration for **6a** and **6a-D_6** was 0.0145 M in CD_3OD. NMR spectra were recorded at 10 min intervals for the first 1 h, and subsequent measurements were taken at 60 min intervals until conversion to **3a** and **3a-D_6** was deemed to be complete, as indicated by the loss of all proton signals from the starting material and emergence of new resonances correlating to the protons of complexes **3a** and **3a-D_6**. The concentrations of complexes **6a** and **6a-D_6** were determined by integration of the Cp* signals of **6** and **3** present in the spectra. As the concentration of **6** fell below 0.0045 M, the signal-to-noise ratio of the Cp* resonances of **6** decreased and integration data lacked accuracy. Therefore, measurements recorded after this concentration had been reached were omitted; hence, the data do not proceed to 100% conversion.

Computational Details. Geometry optimizations have been performed with the Gaussian09 package at the B3PW91 level of hybrid density functional theory.[28] The iridium atom was represented by the relativistic effective core potential (RECP) from the Stuttgart group and the associated basis sets,[29] augmented by an f polarization function.[30] The chlorine atom was represented by RECP from the Stuttgart group and the associated basis set,[31] augmented by a d polarization function.[32] The remaining atoms (C, H, N, O) were represented by a 6-31G(d,p) basis set. The solvent (acetonitrile or methanol) influence was taken into consideration through single-point calculations on the gas-phase optimized geometry with SCRF calculations within the SMD model.[33] For the SCRF calculations the pseudopotential was kept on Ir and all of the remaining atoms were treated with 6-311+G(d,p) basis sets. Influence of the dispersion forces was considered by computing the D3(BJ) corrections as described by Grimme.[34] All energies reported in the present work are Gibbs free energies obtained by summing the SMD energy, the gas-phase Gibbs

DOI: 10.1021/om501197g
Organometallics XXXX, XXX, XXX–XXX

contribution at 353 K (or at 298 K when specified), and the D3(BJ) correction. The NBO analysis was carried out, using NBO 6.0,[35] on wavefunctions computed with B3PW91 in the gas phase with SDDALL for Ir and the 6-31G(d,p) basis set for the other atoms.

Crystallographic Details. Crystal data for complex **2c** were collected by using an Agilent Technologies SuperNova A diffractometer fitted with an Atlas detector using Mo Kα radiation (0.71073 Å). A complete data set was collected, assuming that the Friedel pairs are not equivalent. An analytical numeric absorption correction was performed.[36] The structure was solved by direct methods using SHELXS-97[37] and refined by full-matrix least-squares fitting on F^2 for all data using SHELXL-97.[37] Hydrogen atoms were added at calculated positions and refined by using a riding model. Their isotropic temperature factors were fixed to 1.2 times (1.5 times for methyl groups) the equivalent isotropic displacement parameters of the carbon atom to which the H atom is attached. Anisotropic thermal displacement parameters were used for all non-hydrogen atoms. Crystallographic details are compiled in the Supporting Information (Table S4). CCDC number 1034414 contains supplementary crystallographic data for this paper. These data can be obtained free of charge from the Cambridge Crystallographic Data Centre via www.ccdc.cam.ac.uk/data_request/cif.

■ ASSOCIATED CONTENT

Supporting Information

Text, figures, tables, and CIF and xyz files giving synthetic procedures for starting materials, details on computational analyses, kinetic measurements, crystallographic studies, and ^{1}H and ^{13}C NMR spectra of **5a** and both isomers for **6a**. This material is available free of charge via the Internet at http://pubs.acs.org.

■ AUTHOR INFORMATION

Corresponding Authors

*E-mail for E.C.: eric.clot@univ-montp2.fr.

*E-mail for M.A.: martin.albrecht@ucd.ie.

Notes

The authors declare no competing financial interest.

■ ACKNOWLEDGMENTS

We gratefully acknowledge financial support from the European Research Council (ERC 615653), COST Action CM1205.

■ REFERENCES

(1) (a) Crabtree, R. H. *Chem. Rev.* **1985**, *85*, 245. (b) Shilov, A. E.; Shul'pin, G. B. *Russ. Chem. Rev.* **1987**, *56*, 442. (c) Periana, R. A.; Taube, D. J.; Gamble, S.; Taube, H.; Satoh, T.; Fujii, H. *Science* **1998**, *280*, 560. (d) Labinger, J. A.; Bercaw, J. E. *Nature* **2002**, *417*, 507. (e) Choi, J.; Roy MacArthur, A. H.; Brookhart, M.; Goldman, A. S. *Chem. Rev.* **2011**, *111*, 1761. (f) Caballero, A.; Despagnet-Ayoub, E.; Diaz-Requejo, M. M.; Diaz-Rodriguez, A.; Gonzalez-Nunez, M. E.; Mello, R.; Munoz, B. K.; Ojo, W.-S.; Asensio, G.; Etienne, M.; Perez, P. J. *Science* **2011**, *332*, 835. (g) White, C. M. *Science* **2012**, *335*, 807. (h) Murai, S. (ed.), *Top. Organomet. Chem.* **1999**, *3*, 1. (i) *Activation and Functionalization of C-H Bonds*; Goldberg, K. I., Goldman, A. S., Eds.; American Chemical Society: Washington, DC, 2004; ACS Symposium Series *885*. (j) *Alkane C−H Activation by Single-Site Metal Catalysis*; Perez, P. J., Ed.; Springer: Berlin, 2012.

(2) (a) Jones, W. D.; Feher, F. J. *Acc. Chem. Res.* **1989**, *21*, 91. (b) Arndtsen, B. A.; Bergman, R. G.; Mobley, T. A.; Peterson, T. H. *Acc. Chem. Res.* **1995**, *28*, 154. (c) Stahl, S. S.; Labinger, J. A.; Bercaw, J. E. *Angew. Chem., Int. Ed.* **1998**, *37*, 2180. (d) Shilov, A. E.; Shul'pin. *Chem. Rev.* **1997**, *97*, 2879. (e) Crabtree, R. H. *J. Chem. Soc., Dalton Trans.* **2001**, 2437. (f) Crabtree, R. H. *J. Organomet. Chem.* **2004**, *689*, 4083. (g) Chen, M.; White, M. C. *Science* **2007**, *318*, 783.

(3) For more recent advances in transition-metal-mediated C−H activation, see: (a) Webb, J. R.; Burgess, S. A.; Cundari, T. R.; Gunnoe, T. B. *Dalton Trans.* **2013**, *42*, 16646. (b) Balcells, D.; Clot, E.; Eisentstein, O. *Chem. Rev.* **2010**, *110*, 749. (c) Chen, D. Y.-K.; Youn, S. W. *Chem. Eur. J.* **2012**, *18*, 9452. (d) Li, B.-L.; Shi, Z.-J. *Chem. Soc. Rev.* **2012**, *41*, 5588. (e) Colobert, F.; Wencel-Delord, J. *Chem. Eur. J.* **2013**, *19*, 14010. (f) Schwarz, H. *Angew. Chem., Int. Ed.* **2011**, *50*, 10096. (g) Yeung, C. S.; Dong, V. M. *Chem. Rev.* **2011**, *111*, 1215. (h) Lyons, T. W.; Sanford, M. S. *Chem. Rev.* **2010**, *110*, 1147. (i) Wencel-Delord, J.; Droge, T.; Liu, F.; Glorius, F. *Chem. Soc. Rev.* **2011**, *40*, 4740. (j) Giri, R.; Shi, B.-F.; Engle, K. M.; Maugel, N.; Yu, J.-Q. *Chem. Soc. Rev.* **2009**, *38*, 3242. (k) Colby, D. A.; Bergman, R. G.; Ellman, J. A. *Chem. Rev.* **2010**, *110*, 624.

(4) Janowicz, A. H.; Bergman, R. G. *J. Am. Chem. Soc.* **1982**, *104*, 352.

(5) Allen, K. E.; Heinekey, D. M.; Goldman, A. S.; Goldberg, K. I. *Organometallics* **2013**, *32*, 1579.

(6) Chianese, A. R.; Drance, M. J.; Jensen, K. H.; McCollom, S. P.; Yusufova, N.; Shaner, S. E.; Shopov, D. Y.; Tendler, J. A. *Organometallics* **2014**, *33*, 457.

(7) Maishal, T. K.; Alauzun, J.; Basset, J.; Copéret, C.; Corriu, R. J. P.; Jeanneau, E.; Mehdi, A.; Reyé, C.; Veyre, L.; Thieuleux, C. *Angew. Chem., Int. Ed.* **2008**, *47*, 8654.

(8) Yi, X.-Y.; Chan, K.-W.; Huang, E. K.; Sau, Y.-K.; Williams, I. D.; Leung, W.-H. *Eur. J. Inorg. Chem.* **2010**, 2369.

(9) Young, K. J. H.; Oxgaard, J.; Ess, D. H.; Meier, S. K.; Stewart, T.; Goddard, W. A., III; Periana, R. A. *Chem. Commun.* **2009**, 3270.

(10) (a) Donnelly, K. F.; Petronilho, A.; Albrecht, M. *Chem. Commun.* **2013**, *49*, 1145−1160. (b) Crowley, J. D.; Lee, A.; Kilpin, K. J. *Aust. J. Chem.* **2011**, *64*, 1118−1132. (c) Schulze, B.; Schubert, U. S. *Chem. Soc. Rev.* **2014**, *43*, 2522−2571.

(11) Lalrempuia, R.; McDaniel, N. D.; Müller-Bunz, H.; Bernhard, S.; Albrecht, M. *Angew. Chem., Int. Ed.* **2010**, *49*, 9765.

(12) Woods, J. A.; Lalrempuia, R.; Petronilho, A.; McDaniel, N. D.; Müller-Bunz, H.; Albrecht, M.; Bernhard, S. *Energy Environ. Sci.* **2014**, *7*, 2316.

(13) The geometries of all optimized molecules are given in the Supporting Information in a single xyz file that allows for visualization of the various structures.

(14) Petronilho, A.; Rahman, M.; Woods, J. A.; Al-Sayyed, H.; Müller-Bunz, H.; MacElroy, J. M. D.; Bernhard, S.; Albrecht, M. *Dalton Trans.* **2012**, *41*, 13074.

(15) Hayes, J. M.; Viciano, M.; Peris, E.; Ujaque, G.; Lledós, A. *Organometallics* **2007**, *26*, 6170.

(16) See the Supporting Information for further details.

(17) Arndtsen, B. A.; Bergman, R. G. *Science* **1995**, *270*, 1970.

(18) Strout, D. L.; Zarić, S.; Niu, S.; Hall, M. B. *J. Am. Chem. Soc.* **1996**, *118*, 6068.

(19) Hinderling, C.; Feichtinger, D.; Plattner, D. A.; Chen, P. *J. Am. Chem. Soc.* **1997**, *119*, 10793.

(20) Boutadla, Y.; Davies, D. L.; Macgregor, S. A.; Poblador-Bahamonde, A. I. *Dalton Trans.* **2009**, 5820.

(21) Donnelly, K. F.; Lalrempuia, R.; Müller-Bunz, H.; Albrecht, M. *Organometallics* **2013**, *32*, 8414.

(22) (a) Albrecht, M.; Dani, P.; Spek, A. L.; van Koten, G. *J. Am. Chem. Soc.* **2000**, *122*, 11822. (b) Ryabov, A. D.; van Eldik, R. *Angew. Chem., Int. Ed. Engl.* **1994**, *33*, 783.

(23) Davies, D. L.; Donald, S. M. A.; Al-Duaij, O.; Fawcett, J.; Little, C.; Macgregor, S. A. *Organometallics* **2006**, *25*, 5976.

(24) Lalrempuia, R.; Müller-Bunz, H.; Albrecht, M. *Angew. Chem., Int. Ed.* **2011**, *50*, 9969.

(25) (a) Davies, D. L.; Donald, S. M. A.; Macgregor, S. A. *J. Am. Chem. Soc.* **2005**, *127*, 13754. (b) Gorelsky, S. I.; Lapointe, D.; Fagnou, K. *J. Am. Chem. Soc.* **2008**, *130*, 10848.

(26) Ball, R. G.; Graham, W. A. G.; Heinekey, D. M.; Hoyano, J. K.; McMaster, A. D.; Mattson, B. M.; Michel, S. T. *Inorg. Chem.* **1990**, *29*, 2023.

(27) Fiandanese, V.; Maurantonio, S.; Punzi, A.; Rafaschieri, G. G. *Org. Biomol. Chem.* **2012**, *10*, 1186.

DOI: 10.1021/om501197g
Organometallics XXXX, XXX, XXX−XXX

(28) (a) Frisch, M. J.; Trucks, G. W.; Schlegel, H. B.; Scuseria, G. E.; Robb, M. A.; Cheeseman, J. R.; Scalmani, G.; Barone, V.; Mennucci, B.; Petersson, G. A.; Nakatsuji, H.; Caricato, M.; Li, X.; Hratchian, H. P.; Izmaylov, A. F.; Bloino, J.; Zheng, G.; Sonnenberg, J. L.; Hada, M.; Ehara, M.; Toyota, K.; Fukuda, R.; Hasegawa, J.; Ishida, M.; Nakajima, T.; Honda, Y.; Kitao, O.; Nakai, H.; Vreven, T.; Montgomery, J. A., Jr.; Peralta, J. E.; Ogliaro, F.; Bearpark, M.; Heyd, J. J.; Brothers, E.; Kudin, K. N.; Staroverov, V. N.; Kobayashi, R.; Normand, J.; Raghavachari, K.; Rendell, A.; Burant, J. C.; Iyengar, S. S.; Tomasi, J.; Cossi, M.; Rega, N.; Millam, M. J.; Klene, M.; Knox, J. E.; Cross, J. B.; Bakken, V.; Adamo, C.; Jaramillo, J.; Gomperts, R.; Stratmann, R. E.; Yazyev, O.; Austin, A. J.; Cammi, R.; Pomelli, C.; Ochterski, J. W.; Martin, R. L.; Morokuma, K.; Zakrzewski, V. G.; Voth, G. A.; Salvador, P.; Dannenberg, J. J.; Dapprich, S.; Daniels, A. D.; Farkas, Ö.; Foresman, J. B.; Ortiz, J. V.; Cioslowski, J.; Fox, D. J. *Gaussian 09, Revision B.01*; Gaussian, Inc.: Wallingford, CT, 2009. (b) Becke, A. D. *J. Chem. Phys.* **1993**, *98*, 5648. (c) Perdew, J. P.; Wang, Y. *Phys. Rev. B: Condens. Matter* **1992**, *45*, 13244.

(29) Andrae, D.; Häußermann, U.; Dolg, M.; Stoll, H.; Preuß, H. *Theor. Chim. Acta* **1990**, *77*, 123.

(30) Ehlers, A. W.; Böhme, M.; Dapprich, S.; Gobbi, A.; Höllwarth, A.; Jonas, V.; Köhler, K. F.; Stegmann, R.; Veldkamp, A.; Frenking, G. *Chem. Phys. Lett.* **1993**, *208*, 111.

(31) Bergner, A.; Dolg, M.; Küchle, W.; Stoll, H.; Preuß, H. *Mol. Phys.* **1993**, *80*, 1431.

(32) Höllwarth, A.; Böhme, M.; Dapprich, S.; Ehlers, A. W.; Gobbi, A.; Jonas, V.; Köhler, K. F.; Stegmann, R.; Veldkamp, A.; Frenking, G. *Chem. Phys. Lett.* **1993**, *208*, 237.

(33) Marenich, A. V.; Cramer, C. J.; Truhlar, D. G. *J. Phys. Chem. B* **2009**, *113*, 6378.

(34) (a) Grimme, S.; Ehrlich, S.; Goerigk, L. *J. Comput. Chem.* **2011**, *32*, 1456. (b) Grimme, S.; Antony, J.; Ehrlich, S.; Krieg, H. *J. Chem. Phys.* **2010**, *132*, 154104.

(35) Glendening, E. D.; Badenhoop, J. K.; Reed, A. E.; Carpenter, J. Bohmann, J. A.; Morales, C. M.; Landis, C. R.; Weinhold, F. *NBO 6.0*; Theoretical Chemistry Institute, University of Wisconsin, Madison, WI, 2013.

(36) Clark, R. C.; Reid, J. S. *Acta Crystallogr., Sect. A* **1995**, *A51*, 887−897.

(37) Sheldrick, G. M. *Acta Crystallogr., Sect. A* **2008**, *A64*, 112−122.

DOI: 10.1021/om501197g
Organometallics XXXX, XXX, XXX−XXX